JOURNAL OF MATERIALS SCIENCE 33 (1998) 3255–3266

Biaxial strength of advanced materials

B. J. HULM, J. D. PARKER, W. J. EVANS
Department of Materials Engineering, University of Wales, Swansea SA2 8PP, UK

The concentric ring test has been proposed as the preferred method for testing the flexural strength of bioceramics. If the apparatus used for such tests is proved to be reliable and accurate, it may be adapted to enable cyclic fatigue testing. However, before such adaptions are made, it is necessary to ensure the apparatus operates satisfactorily. The assessment programme involved strain gauge and finite element analyses of both an advanced titanium alloy (IMI 834) and 3 mol % yttria-stabilized zirconia disc specimens and preliminary fatigue tests on IMI 834 discs. The results of the analyses indicate that concentrically loaded discs are exposed to peak biaxial stresses on the tensile surface of the specimen and that these stresses are uniformly distributed within the peak loaded region of the disc. The fatigue response of IMI 834 discs under concentric loading was similar to that under uniaxial tension and torsional loading. The success of this programme will now enable fatigue tests on bioceramic discs to be performed with confidence in the reliability of the test apparatus.

1. Introduction

Bioceramics such as 3 mol % yttria-stabilized zirconia (3Y-TZP) are being considered as the modular component of total hip replacements. These bioceramics exhibit an excellent biocompatibility and high wear resistance. Improvements in the toughness of the material over recent years have encouraged its wider acceptance and research must now consider other performance criteria such as strength and fatigue behaviour.

The standard methods for determining the flexural strength of advanced ceramics had previously been three- and four-point bending [1]. Recently, however, such traditional methods have been replaced by the concentric ring test [2] where disc-shaped specimens are loaded between two coaxial rings of different diameters. The concentric ring test subjects the surface of the material to potentially more damaging biaxial stresses as opposed to uniaxial stresses encountered in other test methods. In addition, a greater surface area of the material is exposed to peak stresses than is the case for the three-point bend, and unlike bar specimens, the flexural strength of the material is not influenced by machine-edge flaws and is thus more reliable in determining the surface strength of a material. The coaxial ring configuration has been used to compare biaxial data for discs and uniaxial data for bar specimens for dense alumina with statistical predictions of strength [3]. The same coaxial loading arrangement was used by Thiemeier and Bruckner-Foit [4] and Chao and Shetty [5] who worked on the failure prediction of discs of alumina nitride, and on the failure probability of discs of alumina and silicon nitride, respectively. The coaxial ring arrangement has also been used by Soltesz [6] to compare the strength of alumina discs with bar specimens subjected to three- and four-point bending with different surface finish. In an earlier publication [7], Soltesz *et al.* also performed a two-dimensional finite element calculation to determine the stress distribution of concentrically loaded discs of alumina.

Under the loading conditions of gait, endoprostheses are exposed to cyclic stresses and it is therefore critically important to determine the long-term cyclic fatigue performance of such materials. As a result, the concentric ring test used for determining the flexural strength of bioceramics, has been adapted for cyclic loading under both ambient and physiological conditions. However, before attempting to generate fatigue data, it is critical to assess the performance of the test apparatus to ensure accurate loading of the bioceramic discs so that all future results are reliable. Details of the testing facility and the initial tests have been published previously [8]. The present paper describes a comprehensive analysis to determine the peak stress and stress distribution across loaded disc specimens using the same apparatus. Such procedures involved strain gauge and finite element analyses. The results from the analyses were compared with the stress determined by the linear plate bending theory [9]. Results of preliminary fatigue tests on discs of IMI 834 are also presented.

2. Experimental procedure

2.1. Material and test apparatus

The materials used in the test programme were disc-shaped specimens of an advanced titanium alloy (IMI 834) and the bioceramic 3Y-TZP (as-fired). The mechanical properties of both specimens are given in Table I. The dimensions of the disc specimens used were 2.0

TABLE I Mechanical properties of IMI 834 and 3Y-TZP

Material	Young's modulus (MPa)	Poisson's ratio	Cyclic yield stress (MPa)
IMI 834	120	0.33	720
3Y-TZP	200	0.3	N/A

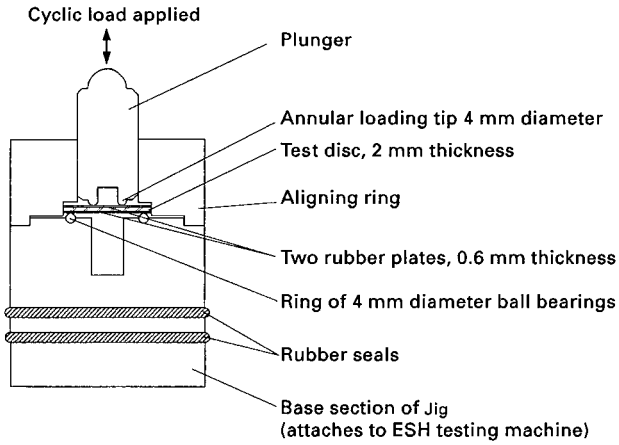

Figure 1 The concentric ring apparatus.

(± 0.1) mm thickness and 36.0 (± 1.0) mm diameter. These dimensions were measured in accordance with the ISO standard [2] using calibrated micrometer gauges.

The concentric ring apparatus is shown in Fig. 1. A disc specimen is placed on a concentric suppport of diameter 30.0 mm, which is comprised of a ring of martensitic stainless steel ball bearings (hardness 192 H_v), each of diameter 4 mm. Accordingly, the base support ring is both resistant to a corrosive environment whilst being sufficiently durable to withstand the transmitted stresses. A plunger with an annular loading tip of diameter 12 mm pushes on to the surface of the disc causing it to flex. Peak biaxial stresses are thus created on the opposite (tensile) face of the disc within the area of the upper loading ring. In order to resist a corrosive environment, the plunger was manufactured from a titanium alloy (IMI 834) which was then subjected to a nitrogen environment to form a hard (650 H_v), surface coating, a property necessary to minimize damage during disc fracture. As required by the ISO standard [2], rubber plates, each of thickness 0.6 mm and Shore hardness 60, sandwich the disc and are used to reduce the effects of any variation in surface flatness. As 3Y-TZP femoral heads are exposed to the potential hazards of a body fluid environment, the apparatus has been adapted for testing discs under simulated physiological conditions by enclosing the test jig within a Perspex thermostatically controlled fluid-filled jacket. A phosphate-buffered Ringer's solution added to the environmental chamber provided the required test environment. The apparatus adapted for environmental testing is shown in Fig. 2.

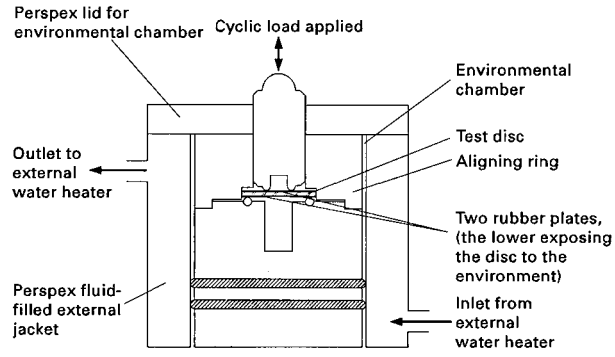

Figure 2 The concentric ring apparatus adapted for environmental testing.

2.2. Test method and analytical procedures

According to the linear plate bending theory [9], a disc loaded in the coaxial ring arrangement is exposed to peak stresses on its tensile surface, within the area of the upper loading ring. In each plane parallel to the surface, an equibiaxial stress state exists within this region such that the circumferential and radial stress components are equal. Thus, by applying Equation 1 and using the appropriate constants for any one disc specimen, at a given load the peak biaxial stress in the disc can be determined as

$$\sigma_{peak} = \frac{3P}{2\pi t^2}\left[(1+\nu)\ln\frac{d_S}{d_L} + (1-\nu)\frac{d_S^2 - d_L^2}{2d^2}\right] \quad (1)$$

where σ_{peak} is the peak biaxial stress applied to the disc (N m^{-2}), P the peak load (N), ν Poisson's ratio for the test material, t the thickness of the specimen (m), d the diameter of the specimen (m), d_S the support ring (mean) contact diameter (m), and d_L the loading ring (mean) contact diameter (m). To ascertain the applicability of Equation 1 to discs used in the present test appparatus, finite element and strain gauge analyses were undertaken. Moreover, both analyses were able to determine the stress distribution in loaded specimens, unlike the theoretical formula which is only able to establish the peak stress.

2.2.1. Finite Element Analysis

A finite element analysis (FEA) was undertaken to determine the stress distribution in concentrically loaded disc specimens of both IMI 834 and 3Y-TZP. The model was run on an "in-house" three-dimensional small strain elastic–plastic finite element package. The package was originally written to solve elastic–plastic fracture problems and was validated against numerous analytical crack solutions, notably the Sneddon solution [10] for a penny-shaped crack and the work by Pickard [11] for one-quarter circular and one-quarter elliptical defects. The Rice solution [12] for a deeply cracked cantilever specimen was used for an elastic–plastic evaluation of the package.

The mesh used to model each disc was constructed of 1296 twenty-noded, isoparametric brick elements with four elements across the thickness of the disc giving a total number of 6333 nodes and 18 999 degrees of freedom. The ball bearing support ring was

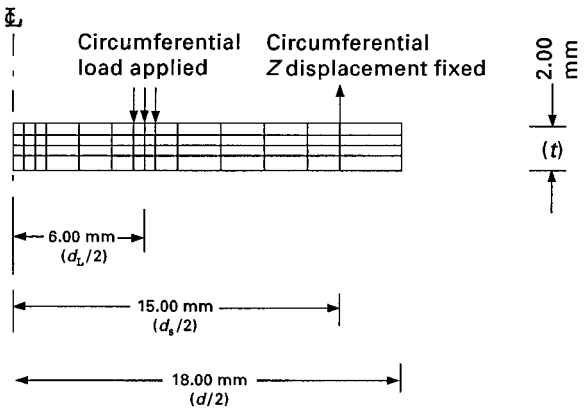

Figure 3 Schematic two-dimensional representation of the FE mesh for a half disc depicting loaded and fixed elements.

modelled by fixing the z displacements of appropriate nodes. Such nodes were on the bottom surface of the mesh and were a radial distance of 15 mm from the centre of the mesh. The annular loading ring was modelled as a 1 mm wide band of mean radius 6 mm. A two-dimensional representation of half the disc model is shown in Fig. 3. To model the applied load of 1 kN, a uniform stress of 26.5 MPa was applied to the area of the disc contacted by the annular loading ring. As 3Y-TZP is a ceramic, it behaves in a linear elastic manner and therefore the results for any other load can be obtained by multiplying the given stresses by the applied load (kN). In the case of IMI 834, the stresses for any elastic load can be obtained in the same manner, provided the yield stress of the material is not exceeded. The material properties used for IMI 834 and 3Y-TZP are given in Table I. In the case of 3Y-TZP, an unrealistic yield stress of $\sigma_y = 5000$ MPa was used to avoid any plasticity. The stress distribution across the tensile surface of each disc was obtained by running the simulation with the disc rotated from a 0° position through 45° and 225° positions.

2.2.2. Strain gauge analysis

In order to determine the stresses in discs loaded in the present concentric ring apparatus, a strain gauge analysis (SGA) was conducted on three disc specimens. The analysis was undertaken to:

(a) determine the peak circumferential and radial stress components in a loaded disc;

(b) establish whether discs are accurately loaded in the apparatus such that a uniform stress distribution exists within the region of the loading ring;

(c) ascertain whether the measured stresses differ when the discs are loaded in air or in Ringer's solution.

2.2.2.1. Preparation of instrumented discs. In concentrically loaded disc specimens, a biaxial stress state exists and therefore determination of the two stress components required the selection of a strain gauge with a rosette configuration. With the principal directions unknown, three independent strain measurements (in different directions) are necessary to determine the principal strains and stresses. Stringent procedures were followed when preparing the instrumented discs so as not to contaminate the gauges and to ensure their accurate bonding and positioning on the surface of each specimen. Measurements of the principal strains in the area of a disc exposed to peak stresses required the use of a single rosette gauge, whereas two rosette gauges were necessary to determine the stress distribution in this area. A single rosette gauge was bonded to the tensile surface of an IMI 834 and a 3Y-TZP disc specimen. In each case, the centre of the gauge was positioned a radial distance of 2.0 mm from the centre of the disc. As measurements were to be taken in air and in Ringer's solution in the case of the 3Y-TZP disc, the gauge was coated in a silicone rubber to protect the adhesive bonding the gauge to the disc from environmental attack. A further 3Y-TZP disc was prepared with two rosette gauges. These were bonded to the tensile surface at radial distances of 2.5 mm (inner gauge) and 4 mm (outer gauge) from the centre of the disc. The inner gauge measured strains near the centre of the disc and the outer gauge measured them towards the edge of the upper loading ring. The uniformity of stress across this region could therefore be determined.

2.2.2.2. Measurement procedure. Each of the three gauged discs were consecutively positioned in the concentric ring apparatus. The site of the gauges in relation to the loading and support rings is indicated in Fig. 4. For each strain gauge analysis, the apparatus was installed in a computer-controlled servo-hydraulic Instron testing machine and loads applied to the instrumented disc via the upper loading ring. In each case, loads were applied at a rate of 0.05 kN s^{-1} with a dwell period of 3 s for every load increment, to allow each of the three gauges in the rosette to record consecutively the strain at the same load. The recorded strains were converted to stresses by using the appropriate value for Young's modulus.

(a) *Determination of peak stress components.* The SGA was conducted to determine the circumferential and radial stress components of the biaxial stress in

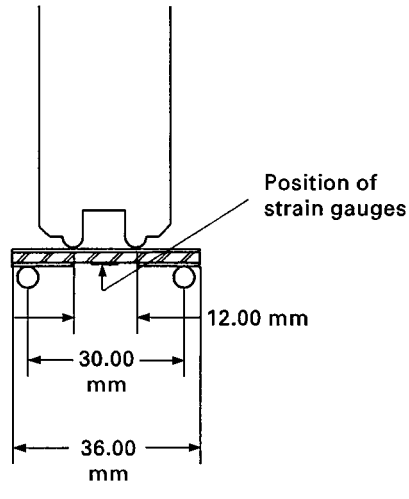

Figure 4 Dimensions of the specimen, loading and support ring.

a disc during loading and to determine the applicability of Equation 1 to discs in the present test apparatus. A single-gauged IMI 834 disc was positioned in the apparatus shown in Fig. 1, and loads ranging from 0–3.42 kN were applied to the disc. The upper load limit was set so as not to exceed the cyclic yield stress of the metal. The measured stresses determined from the analysis were compared with the calculated biaxial stress, obtained from Equation 1.

(b) *Measurement of stress distribution.* The SGA on the double-gauged 3Y-TZP disc specimen enabled the uniformity of stress within the loading ring (tensile surface) to be determined during concentric loading of the disc. With the instrumented disc positioned in the apparatus shown in Fig. 1, loads ranging from 0–1.55 kN were applied to the specimen. The upper load limit was set at this value as the flexural strength of the material is variable due to low flaw tolerance and some specimens are unable to tolerate loads much greater than this. The test was repeated with the disc rotated on the support ring from a 0° position through 90° and finally to a 180° position and measurements of strain recorded and stresses evaluated.

(c) *Measurement of stresses in air and Ringer's solution.* Future disc testing will be conducted in air and in Ringer's solution to determine whether the fatigue strength of 3Y-TZP is reduced in the presence of a physiological environment. It was therefore important to ascertain whether the physical presence of a liquid environment had any effect on the stresses measured on the surface of a loaded disc. The SGA was conducted on the coated, single-gauged 3Y-TZP disc specimen in the apparatus shown respectively in Figs 1 and 2 under both ambient and environmental (Ringer's solution, 20 °C) conditions. Loads ranging from 0–1.503 kN were applied to the instrumented disc for each test and measurements of strain recorded and stresses evaluated.

2.2.3. Cyclic fatigue of IMI 834

Following the analytical procedures, preliminary fatigue tests were conducted on discs of IMI 834 in the apparatus described in this paper. Tests were carried out under ambient conditions using a sinusoidal waveform at a frequency of 5 Hz and stress ratio of 0.1. The data generated for the disc specimens were compared with data previously obtained for the material under unaxial tension and torsional loading [13].

3. Results

3.1. Finite element analysis

The finite element mesh constructed for an IMI 834 disc specimen is shown in Fig. 5. The mesh shows the stress distribution on the tensile surface of the disc under a 1 kN load, applied by a compressive force through the upper loading ring on the opposite face of the disc. The peak stresses lie within the upper loading ring region and appear to be uniform within this area. As indicated, the stress falls away outside this region reaching a minimum towards the peripheral edge of the disc. To clarify the stress distribution across the tensile surface of the disc, a plot of principal stress verses radial distance was constructed with the disc in a 0° position and rotated through 45° and 225° (Fig. 6a). As shown, the peak stresses on the tensile surface of the disc appear uniform within the region of the upper loading ring, i.e. up to a radial distance of 6 mm. Outside this region, the stress falls away such that the stress at the peripheral edge of the disc is only 28% of that at the centre. Closer inspection of the peak stressed region of the disc is presented in Fig 6b. The plot reveals that at a radial distance from 4–5.8 mm, the stress rises above that recorded at the centre of the disc (radial distance 0 mm). The stress reaches a peak at a radial distance of 4.9 mm, but even at this location is only 1.48% greater than that at the centre of the disc. This small rise in stress appears to be due to the influence of the inner edge of the upper loading ring but is small enough to be considered negligible.

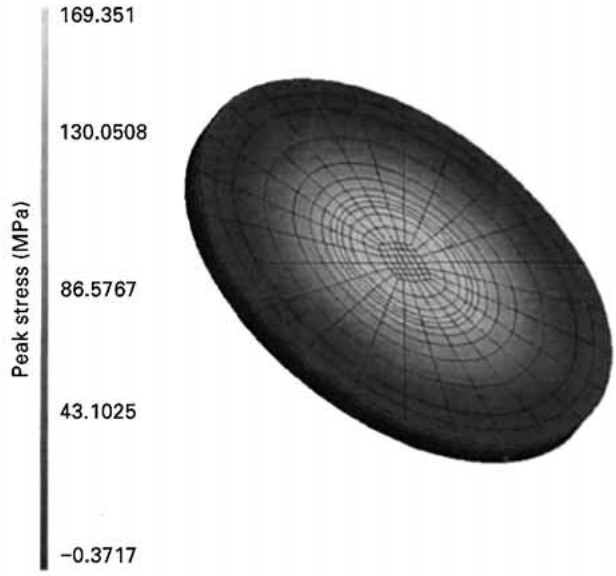

Figure 5 Three-dimensional FE mesh of a disc specimen (tensile surface) under 1 kN load.

Plots of the variation of stress with radial distance for the 3Y-TZP disc subjected to a 1 kN load were constructed in the same manner. Similar observations are noted for the ceramic disc as those for the titanium alloy disc. The variation of principal stress with distance across the disc is presented in Fig. 7a with details of the stress distribution in the region of the loading ring shown in Fig. 7b.

3.2. Strain gauge analysis

3.2.1. Determination of peak stress components

The results for the single-gauged IMI-834 disc are shown in Fig. 8 as a plot of principal stress verses load. As shown, the circumferential and radial stress components of the measured biaxial stress are very similar, differing by less than 3.4%. The measured stress are compared with those calculated for the specimen, according to Equation 1. There is a good agreement between the calculated stress and the peak stress

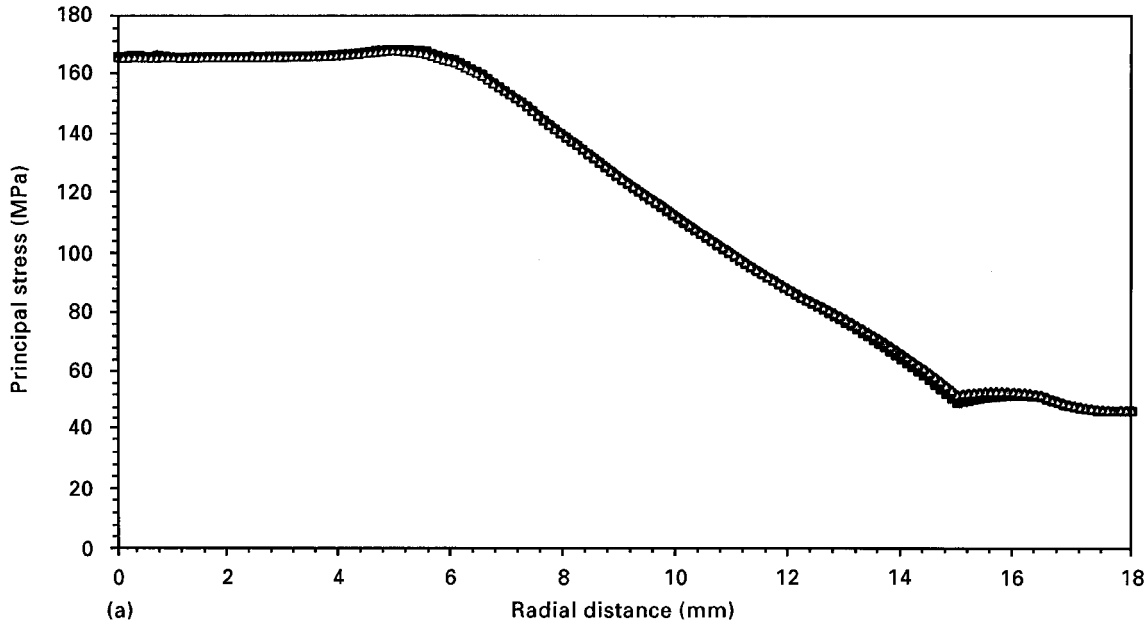

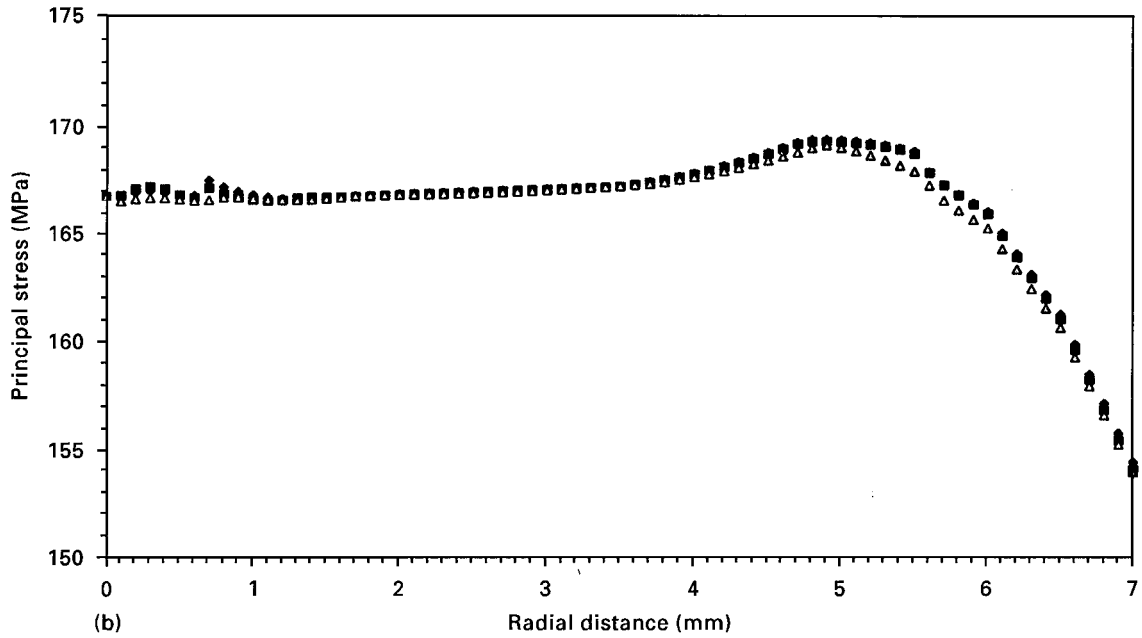

Figure 6 Stress distribution (a) across the tensile surface and (b) within the upper loading ring (tensile surface), of an IMI 834 disc under 1 kN load. (◆) 0°, (■) 45°, (△) 225°.

measured from the surface of the disc, with the maximum difference being less than 2.5%.

3.2.2. Measurement of stress distribution

According to theory [9], a disc subjected to concentric loading should display a uniform stress state on the tensile surface, within the region of the upper loading ring. Therefore, during loading, strain and hence stress measurements recorded from both the inner and outer gauges should be similar. The results for the double-gauged 3Y-TZP disc shown in Fig. 9a, b and c with the disc in 0°, 90° and 180° positions respectively, show this to be true. Although there is a difference of around 8% between circumferential and radial stress components, this appears to be fairly consistent for both inner and outer gauges with the disc in the three different positions. Moreover, the largest difference in peak stress between inner and outer gauges is less than 3.5%. This analysis therefore shows that a uniform stress distribution exists on the tensile surface of a concentrically loaded disc, within the region of the upper loading ring.

3.2.3. Measurement of stresses in air and Ringer's solution

The results of the SGA conducted on a 3Y-TZP disc in air and Ringer's solution are shown in Fig. 10. As with the double-gauged 3Y-TZP disc, the circumferential stress component is again higher than the radial by around 8%, but is again consistent whether the disc is tested in air or in Ringer's solution. However, similar values for the circumferential and radial stresses are

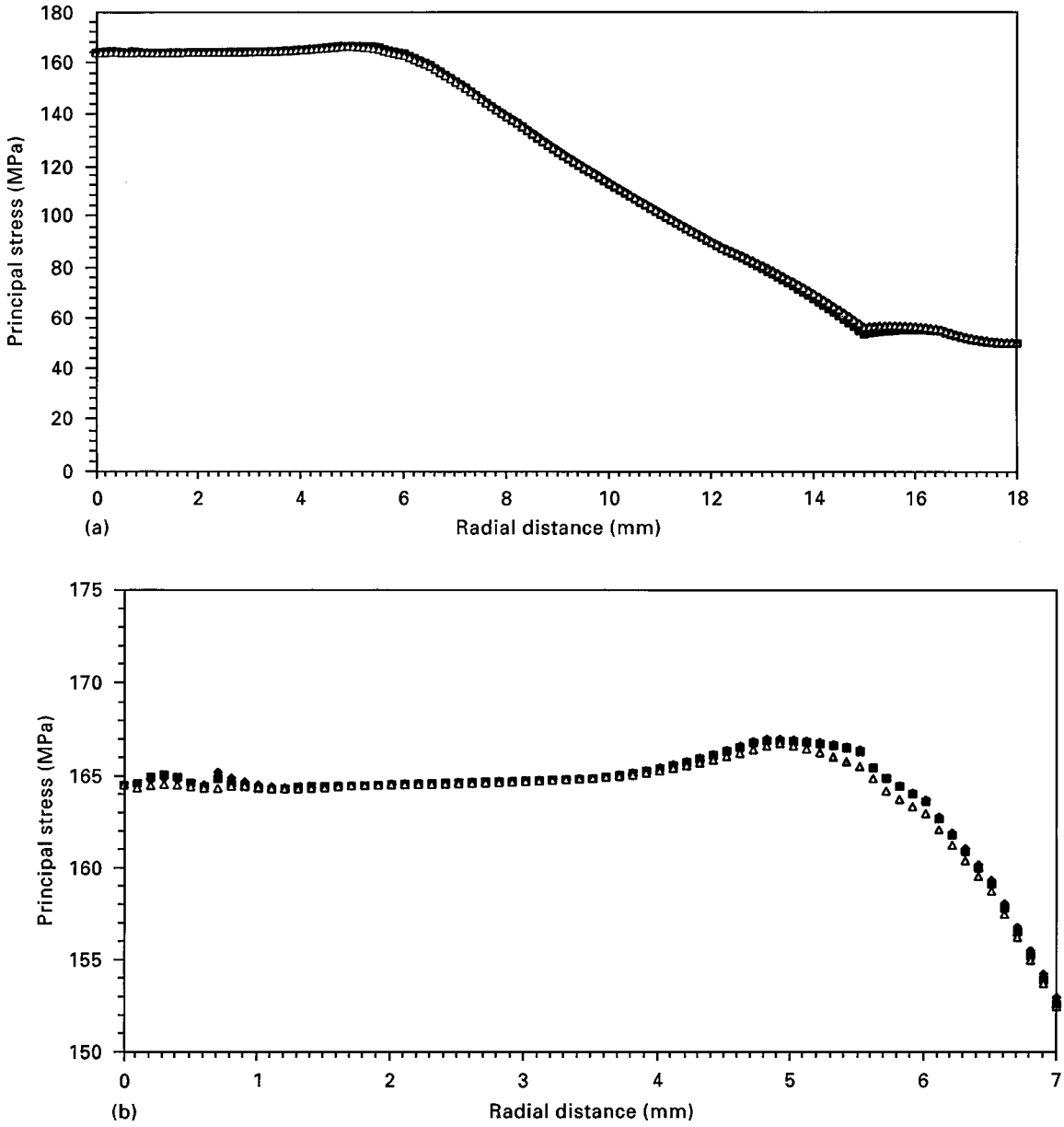

Figure 7 Stress distribution (a) across the tensile surface of 3Y-TZP disc under 1 kN load and (b) within the upper loading ring (tensile surface), of a 3Y-TZP disc under 1 kN load. (◆) 0°, (■) 45°, (△) 225°.

measured with the disc loaded in air or Ringer's solution, differing by less than 4% and 1.4%, respectively. This therefore shows that the presence of Ringer's solution has no significant physical effect on the stresses measured from the surface of a concentrically loaded disc specimen.

3.3. Comparison of calculated and analytical stresses

The dimensions of the disc models constructed for the FEA were the same as those for the discs used in the SGA (single-gauged specimens). Accordingly, the stresses determined from both analyses and those calculated from Equation 1, can be directly compared. The comparison of stresses is shown, respectively, for the IMI 834 disc and the 3Y-TZP disc (single-gauged) in Figs 11 and 12. For the IMI 834 disc, there is an excellent agreement between all three stress determinations with a difference of only 2.4% between the peak measured stress and the calculated stress and less than 0.3% between the calculated stress and that determined from the FEA. Similarly, for the 3Y-TZP disc, there is an excellent agreement between the calculated stresses and those determined by the FEA, with a difference less than 0.13%, and a reasonable agreement between calculated and measured stresses, with a difference of 6.2%.

3.4. Cyclic fatigue of IMI 834

The fatigue data generated for IMI 834 are shown in Fig. 13. The results show a reasonable trend in that the cycles achieved increase with decreasing applied stress. Moreover, the data agree well with those generated under uniaxial tension and torsional loading

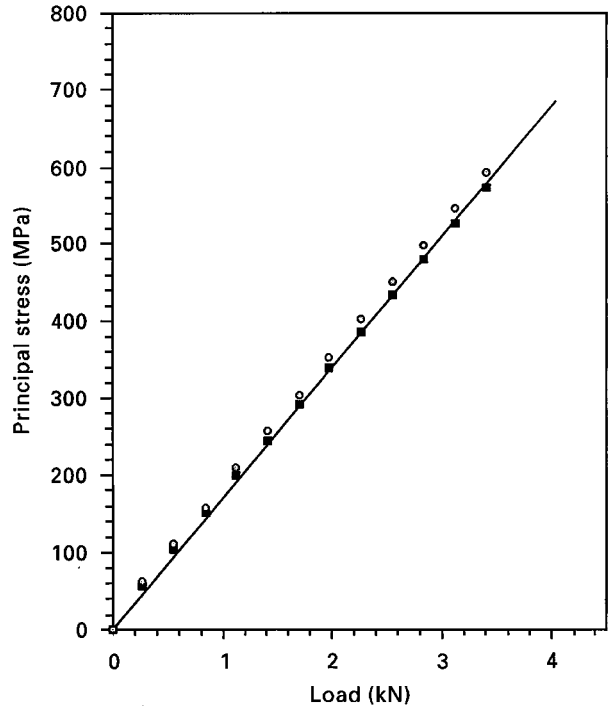

Figure 8 Variation of principal stress with applied load for an IMI 834 strain gauged disc. (■) Radial, (○) circumferential and (–) calculated stress.

conditions, indicating that the concentric ring apparatus is a suitable option for generating fatigue data.

4. Discussion

4.1. Finite element analysis

The FEA conducted on concentrically loaded IMI 834 and 3Y-TZP disc specimens indicated in both cases

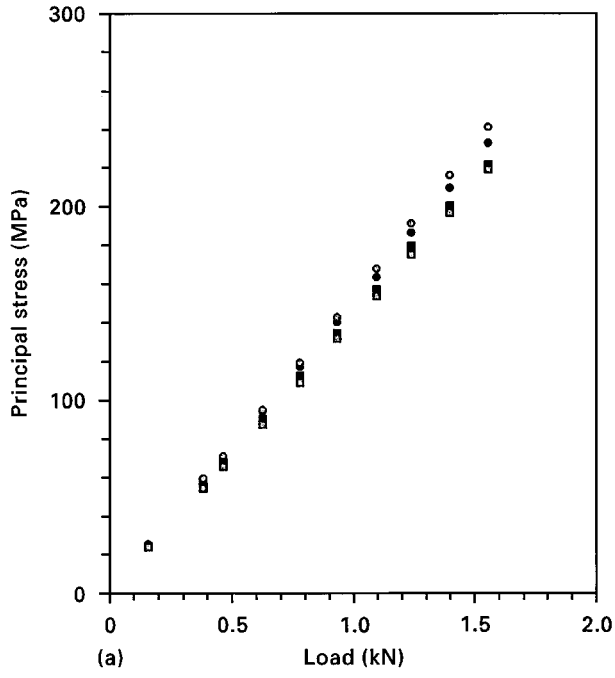

Figure 9 Variation of Principal Stress with Applied Load for 3Y-TZP Strain Gauged Disc in the (a) 0°, (b) 90° and (c) 180° positions. (●, ○) Circumferential and (■, □) radial stress in (●, ■) inner and (○, □) outer regions.

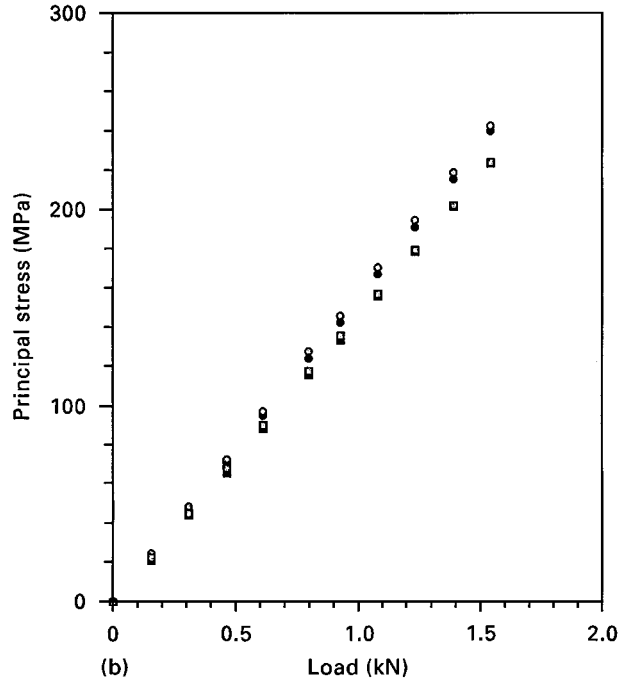

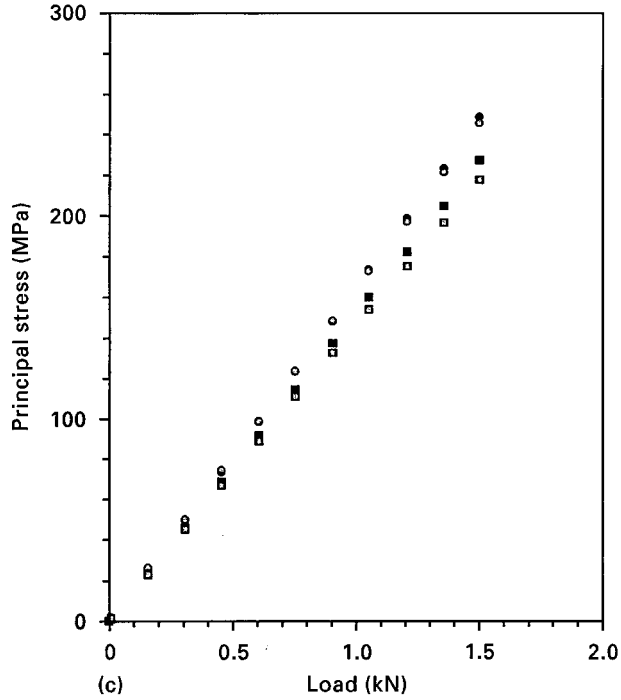

Figure 9 (Continued).

that a uniformly stressed situation existed on the tensile surface within the region of the upper loading ring. This is shown graphically in Figs 6a and 7a, respectively, for IMI 834 and 3Y-TZP. Each plot shows that with the disc rotated through a range of degrees, a uniform peak stress exists within the upper loading ring, i.e. less than a radial distance of 6 mm. Outside this region, the stress falls such that the stress at the peripheral edge of the disc is some 70% lower than that within the upper loading ring. As a result, it is highly unlikely that failure of a concentrically loaded disc would initiate outside the loading ring, even if

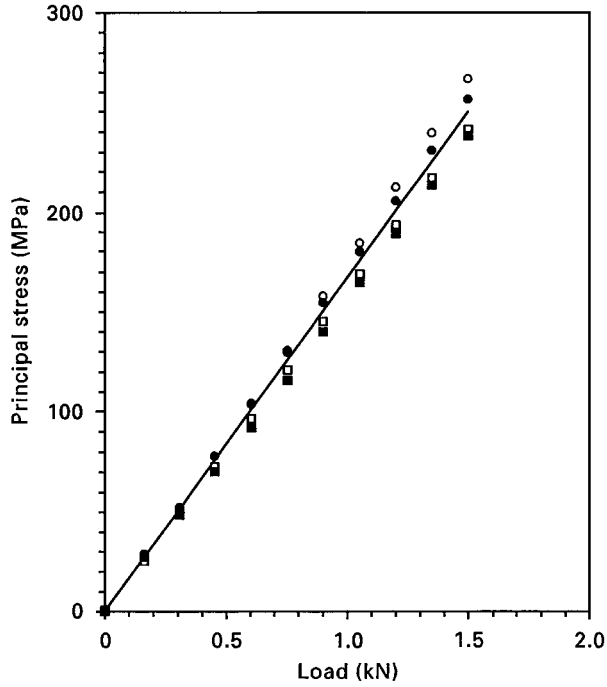

Figure 10 Variation of principal stress with applied load for a 3Y-TZP strain gauged disc. (○, ●) Circumferential and (□, ■) radial stress in (○, □) air and (●, ■) Ringer's solution, (—) Calculated stress.

small edge flaws were present. The small rise in stress noted for both discs at radial distances greater than 4 mm is shown in Figs 6b and 7b. The highest stress noted in both discs, occurring at a radial distance of 4.9 mm, is only 1.48% greater than that at the centre of the disc and appears to be due to the inner edge of the annular loading ring. A similar observation was noted by Soltesz [7] in an axisymmetric finite element analysis on alumina.

4.2. Strain gauge analysis

4.2.1. Determination of peak stress components

The measurements of strain, and hence determination of stress, from a concentrically loaded IMI 834 disc showed that similar values for the circumferential and radial components of the biaxial stress were obtained. Moreover, the peak stress measured from the tensile surface of the disc agreed closely with that calculated from the theoretical formula given in Equation 1. It is therefore evident from the close proximity of measured and calculated stresses that the biaxial stress determined from the theoretical formula, predicts the measured stress with adequate accuracy.

4.2.2. Measurement of stress distribution

The results of the SGA conducted on the double-gauged 3Y-TZP disc show that the stress distribution within the upper loading ring (tensile surface) is uniformly distributed when subjected to concentric loading. This is indicated by the similar stress values evaluated from inner and outer gauges and, as shown in Fig. 9a–c, is consistent when the disc is rotated through a range of degrees, with the maximum difference between the peak stresses being less than 3.3%. The SGA gave true readings on actual specimens loaded in the apparatus and, therefore, the fact that the SGA proved that the stress distribution was uniform, gives complete confidence in the testing facility.

4.2.3. Measurement of stresses in air and Ringer's solution

As 3Y-TZP bioceramic is used as an endoprosthetic material operating under the hostile environment of

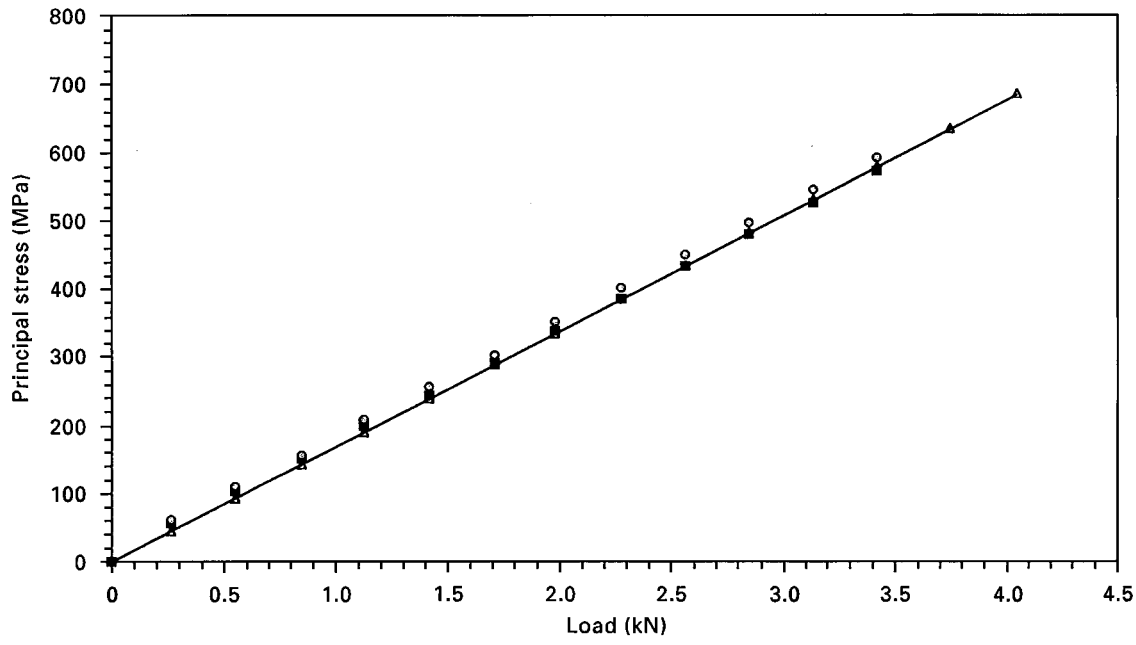

Figure 11 Comparison of (—) calculated and (■, ○, △) analytical stresses in an IMI 834 disc. (■) Radial and (○) circular stress. (△) FE analysis.

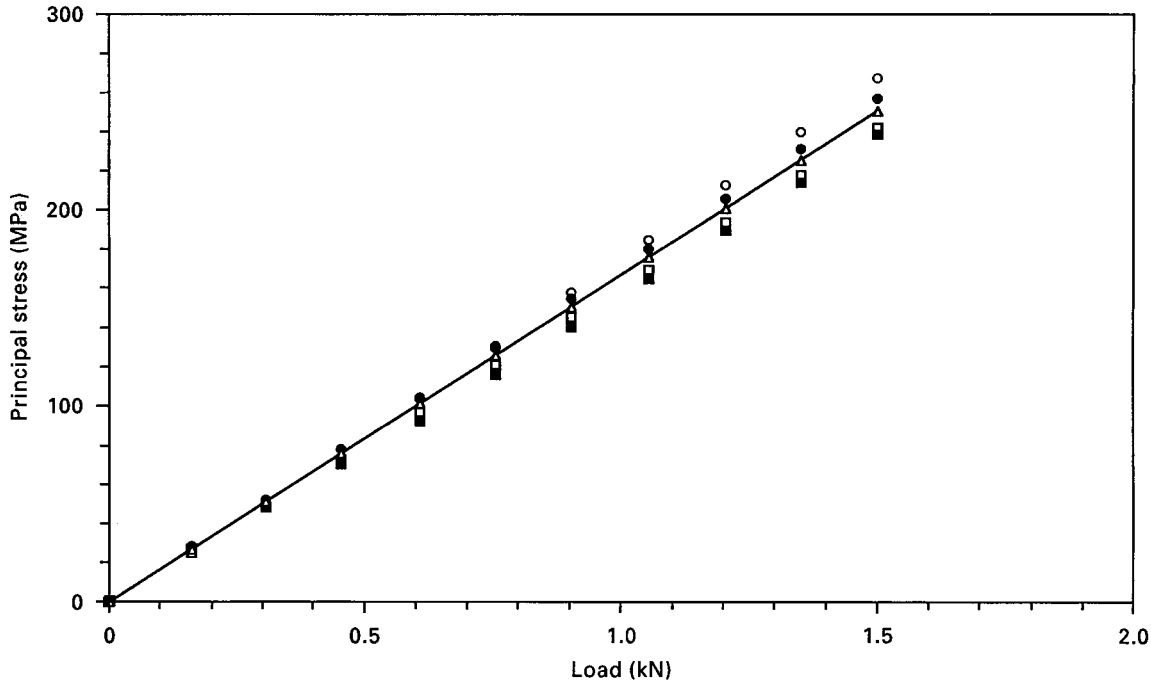

Figure 12 Comparison of (—) calculated and (○, □, ●, ■, △) analytical stresses in a 3Y-TZP disc (single gauged). (○, ●) Circular and (□, ■) radial stress in (○, □) air and (●, ■) Ringer's solution. (△) FE analysis.

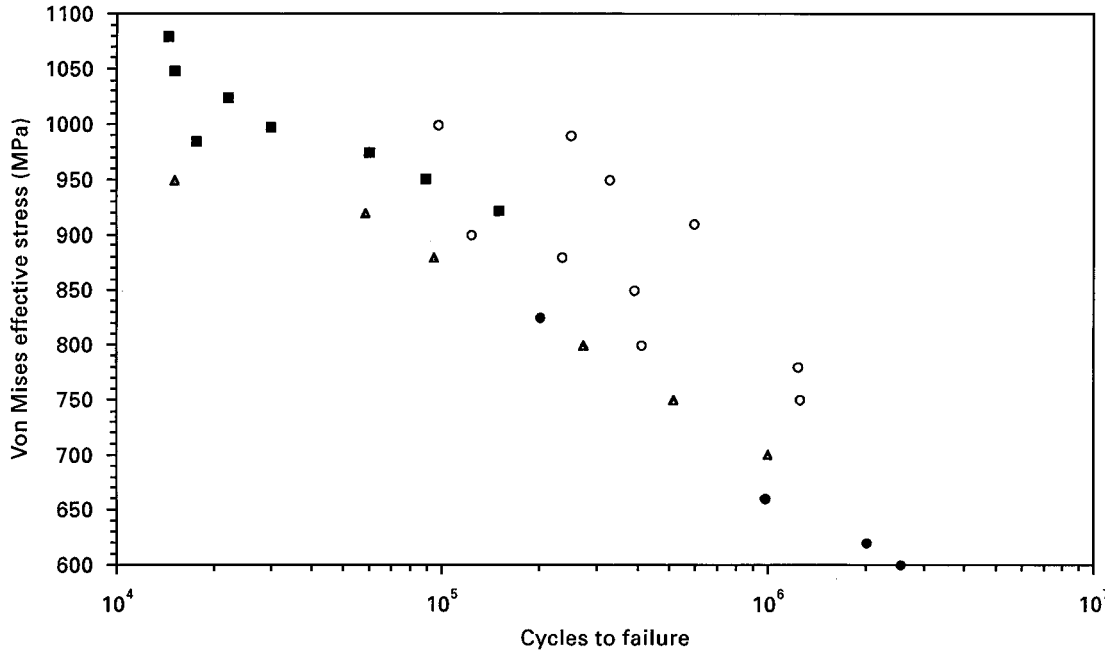

Figure 13 Comparison of cyclic fatigue data using concentric disc loading (biaxial flexion) and data from Evans and Bache [13]. (○) 5Hz, biaxial flexion, (■) 0.2 Hz torsion, (△) 1 Hz tension, (●) 10 Hz tension.

body fluids, it is important to subject test specimens to physiological conditions. There has been concern that the chemical effect of such environments on the material may reduce its strength [14], although further work has shown that the small reduction in strength is not significant enough to warrant concern [15]. As a result of these conflicting views, it is important to perform tests under both ambient and environmental conditions. Therefore, to ensure that the presence of a fluid environment has no physical effect on the stresses encountered by a disc specimen during loading, it was necessary to compare the stresses measured from the surface of a loaded disc in air and when immersed in Ringer's solution. The results of the SGA conducted on the single gauged 3Y-TZP disc (Fig. 10) show that there is a difference between the stress components during loading with the circumferential stress being around 8% higher than the radial. The difference between the stresses is, however, consistent, whether tested in air or Ringer's solution. Moreover, the largest difference between the stresses measured under ambient and environmental conditions is less than 4%. Accordingly, disc testing may be performed under either condition with the confidence that the

physical presence of a fluid environment has no significant effect on the stresses encountered on the surface of a disc.

Also included in Fig. 10 is a plot of the calculated stress, derived from Equation 1. Although the calculated and measured stresses show a reasonable agreement, the most likely explanation for the highest measured stress being some 6.2% greater than the calculated is due to the thickness of the disc specimen. In the case of the titanium alloy disc, thickness measurements taken on a number of specimens were all within the tolerance limit of 2.0 ($\pm$ 0.1) mm and the greatest difference in the thickness of any one sample was only 0.02 mm. Thus the thickness across the whole disc surface is uniformly controlled by precision machining. In the case of the as-fired ceramic, a range of thicknesses was recorded for measurements taken on any one specimen such that the variation was as much as 0.08 mm. In the manufacture of as-fired ceramic discs, there is no grinding operation after sintering and therefore small variations in disc thickness may be encountered. Equation 1 shows that there is an inverse parabolic relationship between the stress and disc thickness, thus a very small drop in thickness results in a substantial rise in stress. Such a relationship is shown graphically in Fig. 14 for a 3Y-TZP disc under a load of 1.5 kN. By re-plotting the calculated stress shown in Fig. 10 and including the calculated values based on the lowest and highest disc thickness, i.e. 1.96 mm and 2.04 mm it can be seen (Fig. 15) that the measured stresses agree more closely with the calculated values based on the smaller thickness value. The difference between the calculated and measured value has now reduced to only 2.3%, which is similar to that for the IMI 834 disc. Therefore, if the strain gauge was on a region of the disc which was locally thinner than the average thickness of the disc, the measured and calculated values agree very closely.

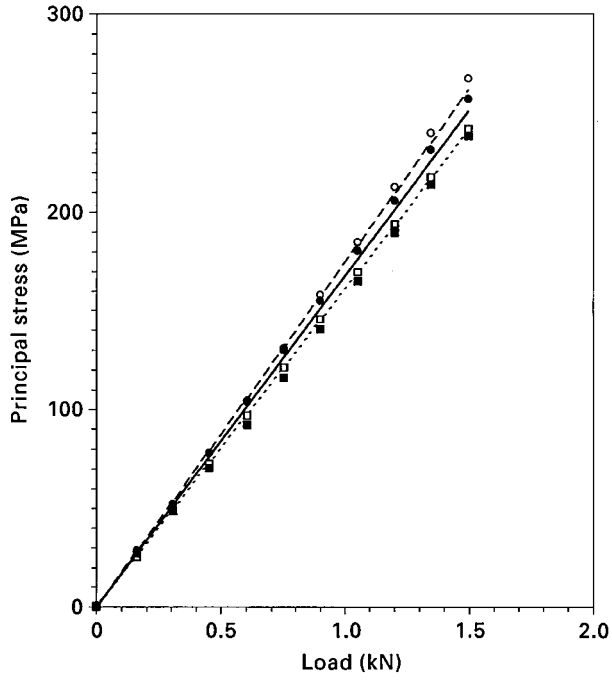

Figure 15 Influence of disc thickness on calculated stress. (○, ●) Circumferential and (□, ■) radial stress in (○, □) air and (●, ■) Ringer's solution. Calculated stresses for t = (——) 2 mm, (- - -) 1.96 mm, and (...) 2.04 mm, are also shown.

4.3. Comparison of calculated and analytical stresses

The finite element mesh for both the IMI 834 and the 3Y-TZP disc were constructed using the same dimensions as the equivalent discs in the SGA. As a result, the stresses determined from the FEA could be directly compared with those measured in the SGA and calculated from the theoretical formula. A comparison of stresses is shown for IMI 834 and 3Y-TZP, respectively, in Figs 11 and 12. In the case of the IMI 834

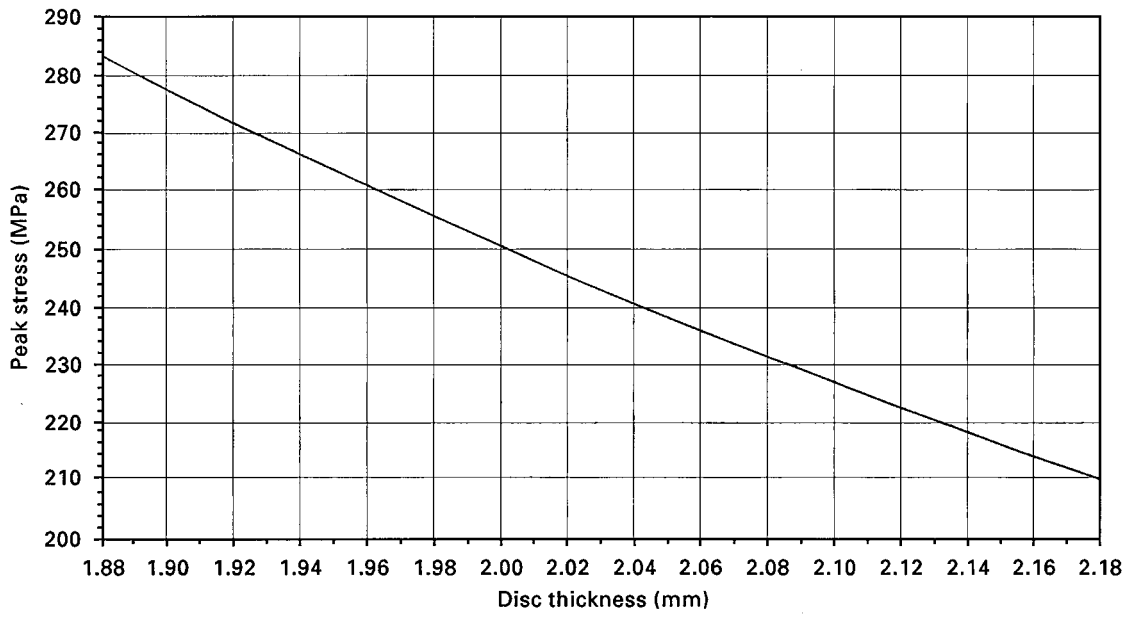

Figure 14 Variation of peak stress with disc thickness for 3Y-TZP (applied load = 1.5 kN).

disc, the stresses from both the FEA and SGA are in close agreement with each other and those calculated from Equation 1. This level of agreement therefore provides confidence in the mechanical performance of the present concentric ring apparatus and that stress values for all future testing of discs can be based on the theoretical formula with the knowledge that it accurately describes the true stress exhibited on the surface of a concentrically loaded disc. For the 3Y-TZP disc, whilst the stresses determined by FEA and the theoretical formula are in close agreement, the stresses measured from the surface of the disc are some 6% greater under a 1.503 kN load. The explanation for this discrepancy is based on disc thickness. If the strain gauge was positioned on a locally thinner part of the disc, the stresses measured at this point would be greater than those determined from Equation 1 using the average thickness value. To ensure an accurate thickness value is used to determine the correct stress in future disc testing of as-fired ceramics , it would be advisable to take an average thickness value of at least five measurements using a point micrometer gauge.

4.4. Cyclic fatigue of IMI 834

The fatigue lives for IMI 834 disc specimens (Fig. 13) show a similar trend to the specimens subjected to uniaxial and torsional loading, obtained from Evans and Bache [13]. The data for the disc specimens, however, show a larger degree of scatter and is likely to be as a result of sensitivity to surface finish, the surface of the discs being ground to remove the central machining pip prior to loading. In addition, although the fatigue response is similar, the data for the disc specimens are displaced to slightly longer lives as appreciable crack growth occurred ($\sim$20 mm) before the discs were classified as failed. Thus, the number of cycles achieved included both crack initiation and propagation. Nevertheless, the results clearly show that the concentric ring test is a suitable option for determining the fatigue life of a material and unlike the metallic material, extended lives due to crack propagation will not occur in 3Y-TZP due to the relatively small critical crack size which will result in catastrophic failure of the disc at crack initiation.

5. Conclusions

1. The circumferential and radial stress components of the biaxial stress, measured from the surface of a concentrically loaded IMI 834 disc, are in close agreement with each other and the stresses calculated from the theoretical formula.

2. The stress distribution across the tensile surface of a concentrically loaded disc is uniform, as indicated by the SGA and FEA, for both IMI 834 and 3Y-TZP. The small rise in stress at a radical distance between 4 and 5.8 mm appears to be due to the influence of the inner edge of the annular loading ring.

3. The stress around the peripheral edge of a concentrically loaded disc is far lower (by $\sim$70%) than that towards the centre, as determined by the FEA. Failure is thus unlikely to initiate outside the loading ring. As a result, small edge flaws on disc specimens are unlikely to influence test results.

4. As indicated by the SGA, the stresses measured from the surface of a 3Y-TZP disc are similar whether loaded in air or Ringer's solution. The liquid environment therefore has no significant physical effect on the stresses measured from the surface of a concentrically loaded disc. Fatigue tests can therefore be conducted in both air and Ringer's solution with the knowledge that the stresses on a disc at a given load are equivalent for both environments. Therefore, any reduction in fatigue life of the material will be as a result of the chemical nature of the test environment.

5. In the case of the bioceramic disc, the higher stresses recorded from the SGA, compared with those determined from the FEA, and the theoretical formula, are likely to be due to the disc being locally thinner at the site of the strain gauge.

6. The trend in cyclic fatigue life for IMI 834 discs subjected to concentric loading, is similar to that when the material is subjected to both uniaxial tension and torsional loading. Therefore, disc testing in the concentric ring apparatus is a suitable option for determining the fatigue life of a material.

7. The performance of the concentric ring apparatus used for subjecting bioceramic discs of biaxial stresses has been fully assessed and the practical and analytical observations agree with the theory. Confident with the mechanical aspects of the apparatus, further adaptions have been made to enable cyclic loading of disc specimens. The cyclic fatigue performance of 3Y-TZP, under a variety of test conditions, is currently being investigated.

Acknowledgement

One of the authors (B. J. H.) is grateful to the EPSRC for provision of a research studentship. She would also like to thank Dr P. Nicholas for constructing the F. E. meshes, Dr M. R. Bache for his advice with the fatigue tests, and Dr S. Spence for his assistance in the work involved in the strain gauge tests.

References

1. "Standard Test Method for Flexural Strength of Advanced Ceramics at Ambient Temperature", ASTM C1161-90 (American Society for Testing and Materials, Philadelphia, PA, 1990).
2. ISO/TC 150/SCI, Draft International Standard, "Implants in Surgery - Ceramic Materials Based on Yttria-Stabilized Tetragonal Zirconia" (1996).
3. M. N. GIOVAN and G. SINES, *J. Am. Ceram. Soc.* **62** (1979) 510.
4. T. THIEMEIER and A. BRUCKNER-FOIT, *ibid.* **74** (1991) 48.
5. L. CHAO and D. K. SHETTY, *ibid.* **74** (1991) 333.
6. U. SOLTESZ, in "Proceedings of the 2nd International Symposium on Ceramics in Medicine", Heidelberg, Germany (1989), *Bioceramics* **2**.
7. U. SOLTESZ, H. RICHTER and R. KIENZLER, in "High Tech. Ceramics", edited by P. Vincenzini (Elsevier Science Publishers B.V. Amsterdam, 1987) p. 149.
8. B. J. HULM, J. D. PARKER and W. J. EVANS, in "Proceedings of the 11th Irish Materials Forum Conference", "Key Engineering Materials", edited by P. E. McHugh (Transtec, Switzerland, 1996) p. 321.

9. E. J. HEARN, in "Mechanics of Materials", Vol. 2, (Pergamon, Oxford, 1985) p. 636.
10. I. N. SNEDDON, *Proc. R. Soc. Lond. Ser. A* **187** (1946) p. 229.
11. A. C. PICKARD, in "The Application of Three Dimensional Finite Element Methods to Fracture Mechanics and Fatigue Life Prediction" (Published by Engineering Advisory Services Ltd., Warley, U.K., 1986) p. 89.
12. J. R. RICE, in "Fracture: Mathematical Analysis of the Mechanics of Fracture. An Advanced Treatise", Vol. 2, edited by H. Liebowitz (Academic Press, New York, 1968) pp. 19–311.
13. W. J. EVANS and M. R. BACHE, in "Proceedings of the 8th World Conference on Titanium", edited by P. A. Blenkinsop, W. J. Evans and H. M. Flower (The Institute of Materials, London, U.K., 1995) p. 1339.
14. J. L. DRUMMOND, *J. Am. Ceram. Soc.* **72** (1989) 675.
15. B. CALES and Y. STEFANI, *J. Mater. Sci. Mater. Med.* **5** (1994) p. 376.

Received 24th June 1997
and accepted 22 April 1998